Designing Anti-Icing Surfaces by Controlling Ice Formation

Xiaoteng Zhou, Yuling Sun,* and Jie Liu*

Understanding the formation of ice from supercooled water on a surface is a matter of fundamental importance and general use. Kinetics of ice nucleation and ice growth on solid surfaces are actively studied, based on which effective anti-icing surfaces are designed. This review introduces one major breakthrough of experimental estimation of the critical ice nucleus size in heterogenous ice nucleation (HIN). Besides that, targeted anti-icing strategies are summarized according to the icing steps: suppression of ice nucleation, regulation of ice growth, and reducing ice adhesion. Factors such as crystal lattice match, charge, and ions, etc., are found to have determined effects on the HIN in specific circumstances. This promotes the study of surfaces with ice nucleation inhibition properties. Recent research about distinct ice growth patterns on hydrophobic and hydrophilic surfaces provides a new insight of designing icephobic surfaces by regulating ice growth or spreading processes. At last, effective surfaces including lubricated surface, low interfacial toughness surface, and superhydrophobic surface are developed to significantly reduce ice adhesion strength. The robustness, cost, and manufacture complexity can be problems that need to be considered for the widespread practice of anti-icing surfaces.

1. Introduction

Unexpected ice formation on surfaces is usually a catastrophe and can lead to economic losses and accidental casualties. Ice on transmission lines can pose a serious threat to the safe operation of power, railways, telecommunication systems, and networks.[1] Ice buildup on aircraft surfaces can reduce performance by up to 50% and can alter flight dynamics parameters, resulting in aircraft crashes.[2] Frost accumulation on the surface of heat transfer units in refrigerators can reduce heat transfer efficiency by up to 70%.[3] Therefore, how to design surfaces that could remain ice-free in subzero temperatures

or could exhibit easy de-icing process is an extremely meaningful issue to be considered.[1d,4]

Though various anti-icing and de-icing strategies have been widely developed, the conventional positive de-icing methods are usually inefficient, high waste and cost, or environmentally unfriendly.[5] To fundamentally and effectively address the problem of superficial icing, understanding and controlling the icing process on the surfaces will facilitate the design of anti-icing surfaces.[1c,d,4,6] Ice forms on solid surfaces mainly through four routes: freezing of supercooled sessile droplets,[7] freezing of impacting supercooled water droplets,[8] frosting,[9] and ice deposition (**Scheme 1**).[10] In winter, when the supercooled drops impact on a surface, freezing happens in short time as the surface temperature is subzero. The freezing of supercooled water or vapor on solid surfaces usually experiences steps of reversible formation of ice nuclei,[4a,11] irreversible growth of ice crystal,[12]

and ice recrystallization.[13] Besides freezing from water or vapor, ice sometimes deposits directly on the solid surface by snowfall.

Efforts have been made to understand the mechanism of ice formation, and various anti-icing and de-icing strategies have been developed with respect to the different routes of ice formation (Scheme 1). For sessile droplet freezing, surfaces with specific charges,[7c,14] ions,[15] or wetting properties,[7b,16] etc., have been applied to inhibit or delay ice nucleation. The freezing of impacting droplet can be solved by employing liquid-repellent surface to inhibit droplet attachment and reducing contact time before bouncing.[17] Frost formation process occurs when water condensation or water vapor desublimation happens on the surface. It can be, respectively, hindered by the timely removal of the condensate droplets due to their high mobility on superhydrophobic surfaces or local icing by spatially controlling the nucleation and the growth modes of ice crystals on surfaces.[9b,12c,18] If ice is inevitably deposited on the surface, the introduction of a aqueous or organic lubricant layer on the surface can effectively reduce its adhesion.[4b,19]
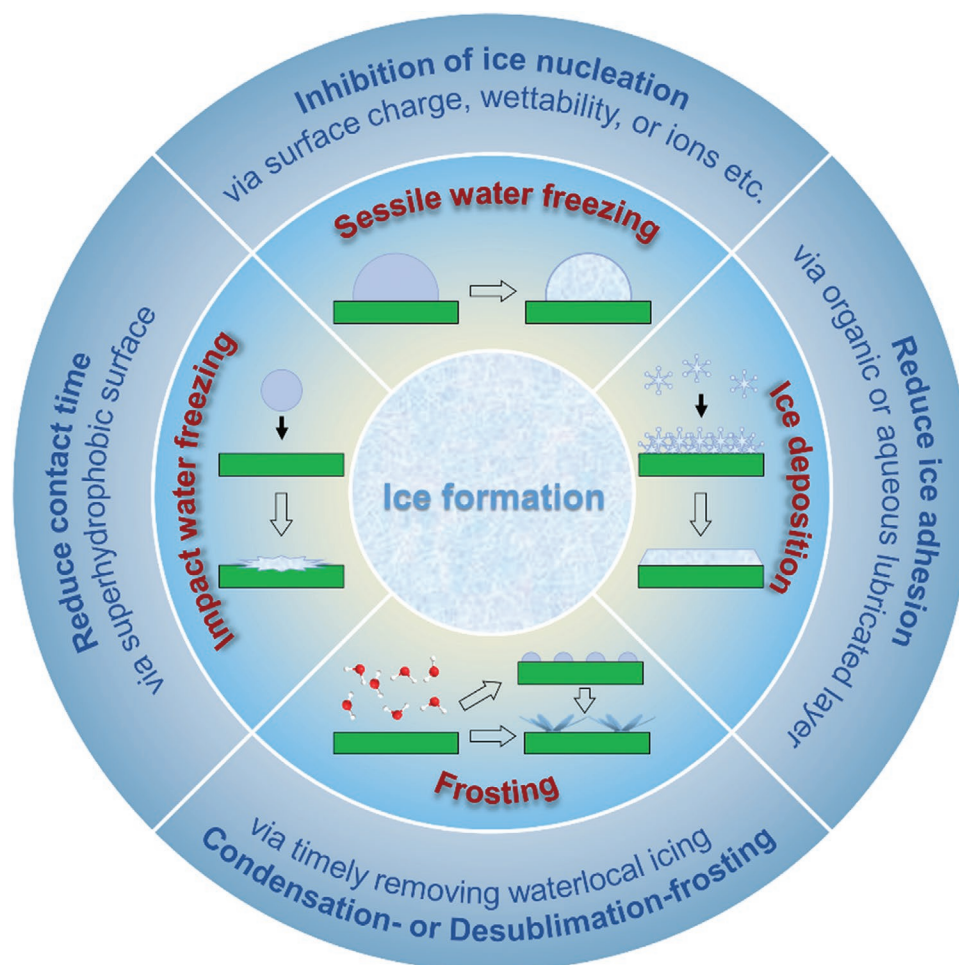
In this review, we briefly summarize the current progress of studies on the regulation of the heterogenous ice nucleation and growth, respectively. Then we correspondingly summarize the anti-icing strategies with respect to the different routes of ice formation. Finally, we discuss the remaining gaps in the field of anti-icing and outlooks for development.

X. Zhou, Dr. Y. Sun, Dr. J. Liu
Max Planck Institute for Polymer Research
Ackermannweg 10, 55128 Mainz, Germany
E-mail: suny@mpip-mainz.mpg.de; liujie@mpip-mainz.mpg.de

The ORCID identification number(s) for the author(s) of this article can be found under https://doi.org/10.1002/admi.202100327.

ADVANCED
SCIENCE NEWS
www.advancedsciencenews.com

ADVANCED
MATERIALS
INTERFACES
www.advmatinterfaces.de

Scheme 1. Icing processes on solid surface. Four routes of ice formation on solid surfaces: freezing of supercooled sessile droplets, freezing of impacting supercooled water droplets, frosting (condensation-frosting or desublimation-frosting), and ice deposition.

2. Heterogenous Ice Nucleation (HIN) on Solid Surface

Ice nucleation in nature proceeds either homogenous or heterogenous modes. The stable ice nucleus is the key to ice formation. With a high nucleation barrier, the homogenous nucleation temperature of water is around 235 K.[20] Therefore, in most cases of ice formation on solid surfaces are originated from heterogenous ice nucleation. Formation of ordered water structure would always be one step before ice nucleus formation.[1d,4a] Specific features existing on solid surfaces, e.g., particle size,[7d,21] crystal lattice match,[22] surface hydroxyl groups,[7e,23] surface defects (e.g., steps, cracks, and cavities),[24] charges,[7c,25] and ions,[26] were found their contributions to the high HIN efficacy by reducing the nucleation barrier. Anti-icing surfaces are accordingly designed based on the understanding of the influences of these features on ice nucleation. However, the main mechanisms of ice nucleation in certain circumstances are still not available. Recently, some new discoveries provide novel approaches and explanations on these remaining issues.

2.1. Size Effect in Heterogeneous Ice Nucleation

Various particles have been attempted to quantify their ice nucleation activity in laboratory experiments.[21b,27] As is previously reported that the size plays a key role in determining the ability of particle to induce ice nucleation when its radius is within the range of 10–1000 Å.[28] It was discovered that both the ice nucleation active surface site (INAS) density and the activated fraction f_{IN} for different INAS densities are related to the particle size. The INAS density represents the number of nucleation sites per unit surface area of the particles, and the activated fraction is the ratio of the cumulative number of sample units frozen at a certain temperature to the original number.[29] In a certain INAS density, the activated fraction usually increases positively with the particle size.[28c]

Recently, graphene oxide nanosheets were found to have ice-nucleation activity.[30] The hydroxy groups on the 2D nanosheet are arranged to match with the ice crystal lattice (**Figure 1**a,b).[31] Benefits from this suitable model systems, Wang et al. succeeded to probe the critical nucleus size by probing the ice nucleation activity of the graphene oxide (GO) nanosheets.[32] They
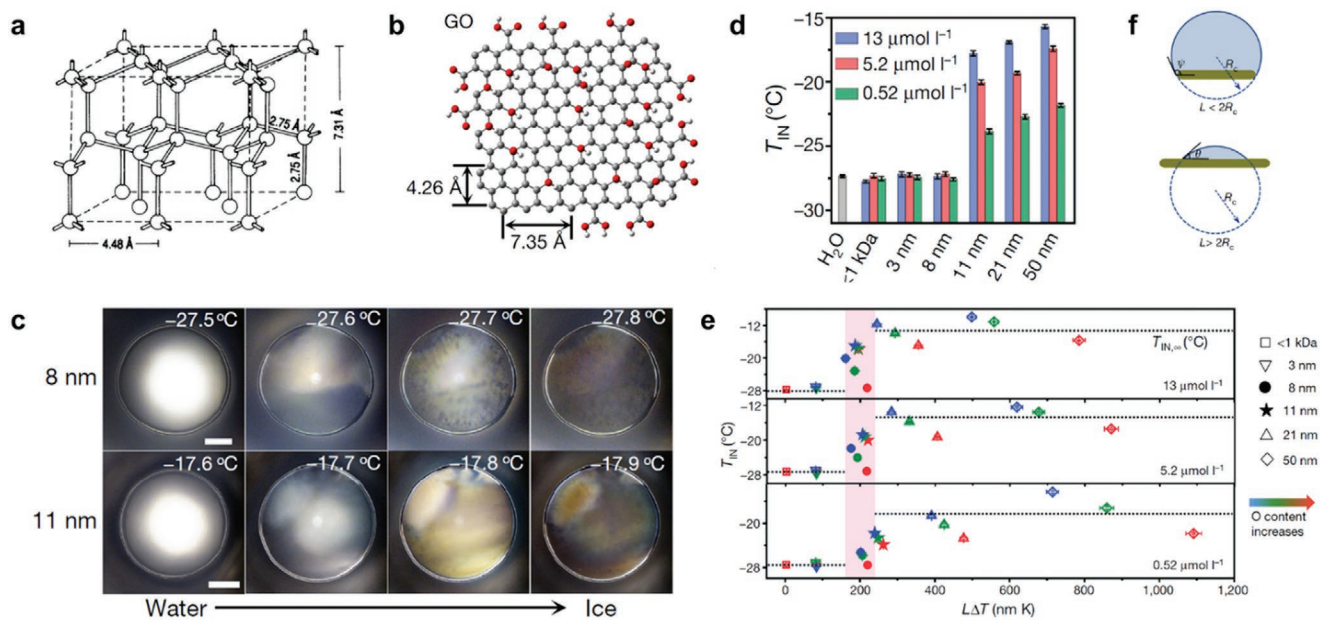
**ADVANCED
SCIENCE NEWS**

www.advancedsciencenews.com

**ADVANCED
MATERIALS
INTERFACES**

www.advmatinterfaces.de

Figure 1. Experimental measurement of critical ice nucleus size for heterogenous ice nucleation. a) Scheme shows the crystal structure of hexagonal ice. Oxygen: ball; O-H···O hydrogen bond: rod. Reproduced with permission.[22c] Copyright 1990, AAAS. b) Illustration of graphene oxide (GO) nanosheets. Carbon, gray; oxygen, red; hydrogen, white. c) Images show the freezing of water droplets (0.2 µL) containing GOs with different sizes. Scale bar: 200 µm. d) Ice nucleation temperatures (T_{IN}) of water droplets (0.2 µL) containing GOs with different sizes. e) The relationship between T_{IN} and $L\Delta T$ (the supercooling scaled size of GOs) for water droplets with different concentrations of GOs with six sizes and three oxidation extents. f) Schemes illustrate the growth of ice nucleus on GOs with different sizes. b–f) Reproduced with permission.[32] Copyright 2019, Springer Nature.

systematically explored the effect of GO sizes within 3–50 nm on ice nucleation (Figure 1c,d). Mean ice nucleation temperatures (T_{IN}) of water droplets containing GOs of different sizes were measured. They found that the T_{IN} of the droplet containing 8 nm GOs (–27.6 °C) is about 10 °C lower than that of a droplet containing 11 nm GOs (–17.9 °C) under otherwise identical experimental conditions. And the following experiments proved that the abrupt change in T_{IN} occurs at $L\Delta T \approx 200$ nm K (L is the average lateral size of GOs, and $\Delta T = T_m - T_{IN}$, with T_m being the equilibrium melting temperature of ice) (Figure 1e). When $L\Delta T < 200$ nm K, ice nucleation is mainly induced by the water–substrate interface. When $L\Delta T > 200$ nm K, T_{IN} is almost independent of the value of $L\Delta T$ but varies with GO concentration, which means GOs are large enough to induce ice nucleation. A model of ice nucleus formation on the GO sheets was proposed (Figure 1f): when $L > 2R_c$ (R_c represents the radius of the critical ice nucleus), the corresponding critical ice nucleus is a spherical cap with a small contact angle sitting on the surface of GO. In contrast, when $L < 2R_c$, the growth of the ice nucleus is limited by the size of GO sheet and thus forms a spherical-like shape. As a result, a higher nucleation barrier occurs on the water-ice transition induced by smaller GO sheets. Their work provides a reliable experimental evidence for a more precise range of critical ice nucleus size for heterogenous ice nucleation. This implies that surfaces with a pattern size comparable to that of the critical ice nucleus can alter a surface's ability to control ice formation. Based on the high nucleation activity of graphene oxide, Joghataei et al. recently found that the heterogenous ice nucleation activity of the graphene–graphene oxide nanoparticles is comparable with the silver iodide (AgI) particles which is commonly used as a high effective ice nucleation agent.[33]

2.2. Ion-Specific Effects in Heterogenous Ice Nucleation

The ion-specific effects were reported to have influence on the dynamics and structures of interfacial water.[34] Though ions are also involved ice formations in various situations, it is still not clear if there is a ion-specific effect of the heterogenous ice nucleation.[35] Giving this, He et al. studied the effect of ionic surface on the ice nucleation with different counter ions of polyelectrolyte brush surfaces.[26] Cationic poly[2-(methacryloyloxy)-ethyltrimethylammonium] (PMETA) and anionic poly(3-sulfopropylmethacrylate) (PSPMA) brushes were used (**Figure 2**a), in which the Cl⁻ in PMETA and K⁺ in PSPMA could be exchanged to diverse counter ions, e.g., SO_4^{2-}, F⁻, Ac⁻, HPO_4^{2-}, and Cl⁻ or Ca²⁺, Mg²⁺, Gdm⁺, K⁺, and Na⁺. When water droplets attach to these polyelectrolyte brush surfaces, a fraction of counter ions are released from the brushes due to the osmotic pressure and form a diffusion layer of counter ions at the brush/water interface (Figure 2a). The HIN temperatures (T_H) on the PMETA-I⁻ brush surfaces show significant difference from the PMETA-SO_4^{2-} brush surfaces (Figure 2b,c). Particularly, the T_H increases in the anion sequence of $SO_4^{2-} <$ F⁻ < Ac⁻ < $HPO_4^{2-} <$ Cl⁻ < Br⁻ < SCN⁻ <NO_3^- < I⁻ on PMETA brush surfaces and in the cation sequence of Ca²⁺< Mg²⁺< Gdm⁺ < K⁺ < Na⁺ < Cs⁺ < TMA⁺ < Li⁺ < NH₄⁺ on PSPMA brush surfaces. Note that all these sequences match well with the Hofmeister series.[26] Through investigating the interactions between PMETA brushes and three representative counter ions, F⁻, Cl⁻, and I⁻, with MD simulations, they found that the fraction of ice-like water molecules typically increases in the order of F⁻ < Cl⁻ < I⁻ (Figure 2d). Thus, induced by the counter ions, the faster the ice-like water forms, the higher the ice nucleation temperature will be on the brush surfaces (Figure 2e).
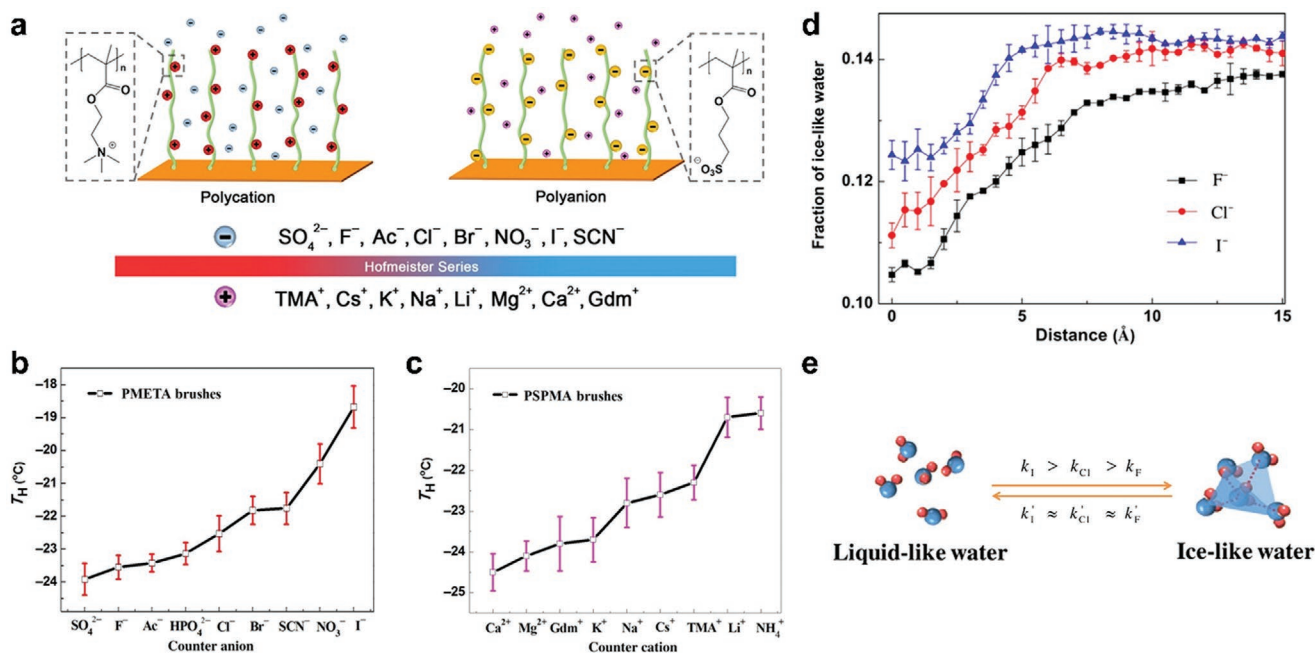
Figure 2. Tuning ice nucleation with counter ions on polyelectrolyte brush surfaces. a) PMETA and PSPMA brushes are used as model surfaces to study the effect of diffused counter ions on tuning HIN. b,c) Distinct efficiency of anions and cations in tuning HIN. d) Fraction of ice-like water molecules (tetrahedrality above 0.9) around PMETA brush with corresponding counter ions of F^{−}, Cl^{−}, and I^{−}. e) Schemes illustrate transition kinetics of liquid-like and ice-like water molecules at the brush/water interface. a–e) Reproduced with permission.[26] Copyright 2016, AAAS.

2.3. Atomic Arrangement-Induced Heterogenous Ice Nucleation

Antifreeze proteins (AFPs) are famous for their unique capabilities of controlling ice formation. Koop et al. reported that AFPs including type-III AFP from fish and T_mAFP from beetles can trigger ice nucleation above the homogenous freezing temperature when their concentration are low in aqueous solutions.[36] In addition, the AFPs can be directly adsorbed to the ice crystal surface by the ice-binding face.[37] The adsorbed AFPs cause curvatures on the ice surface between adjacent AFPs, thereby slow down or stop ice growth by interfering with step propagation across the surface.[38] Compared to AFPs, graphene oxide has the similar binding kinetics to ice surface.[31a] However, the interaction mechanism of the AFPs or graphene oxide to ice surface is still far from clear. Via selectively grafting the ice-binding face (IBF) and the nonice-binding face (NIBF) of AFPs to solid substrates (**Figure 3**), Liu et al. illustrated a janus effect of the AFPs (from M. p. dzungarica, MpdAFP) on ice nucleation.[7e] They tethered MpdAFP on surface by polydopamine (PDA) with NIBF exposed outward and by (3-glycidoxypropyl) methyldimethoxysilane (GOPTS) with IBF exposed outward (Figure 3a). The ice nucleation temperature significantly decreases from −28.0 to −31.0 °C on the NIBF surface when AFPs coverage becomes larger than 80.0% (Figure 3b). In contrast, the IN temperature rapidly increases from −27 to −24.0 °C on the IBF surface when AFPs coverage becomes larger than 64.0% (Figure 3c). Therefore, the NIBF surface depresses the formation of the stable ice nucleus, while the IBF surface facilitates the formation of ice nucleus. According to the following MD simulation, they found the formation of hexagonal ice-like water with a hexagonal hydrogen bond network in the hydration layer induced by the IBF surface (Figure 3d). In contrast, the

water molecules nearby the surface exhibit disordered structure because of irregular arrangement of hydrophobic/hydrophilic groups in NIBF (Figure 3e). Their findings imply a fact that the IBF and the NIBF cooperatively work together to realize the functions of AFPs in suppressing ice formation.

2.4. Others

The crystal lattice match can also influence ice nucleation via induced epitaxial growth of ice. Kiselev et al.[22b] directly observed the aligned ice crystals on certain crystal face of a K-rich feldspars. They proposed that the alignment of ice crystals on the feldspars surface arises from the preferential nucleation of prismatic crystal planes of ice on high-energy (100) surface planes of feldspar. In addition, the surface charge also plays an important role in affecting ice nucleation.[39] Lubomirsky et al. studied the influence of the surface charge on the ice nucleation via a pyroelectric material, on which the surface charge can be artificially regulated to be positive or negative. They found that the surfaces positively charged promote ice nucleation, whereas the same surfaces negatively charged reduce the ice nucleation temperature.[14b] Influences of the surface charges on ice nucleation was also studied by Yang et al. via investigating ice formations dynamics on the supercharged polypeptides (positively charged lysine (K) or negatively charged glutamic acid (E)) modified surfaces.[7e] They found that the positively charged polypeptides facilitate ice nucleation, while negatively charged polypeptides suppress it. By studying the influence of different factors on the ice nucleation process, it is important to provide theoretical guidance for the preparation of effective ice suppression surfaces.
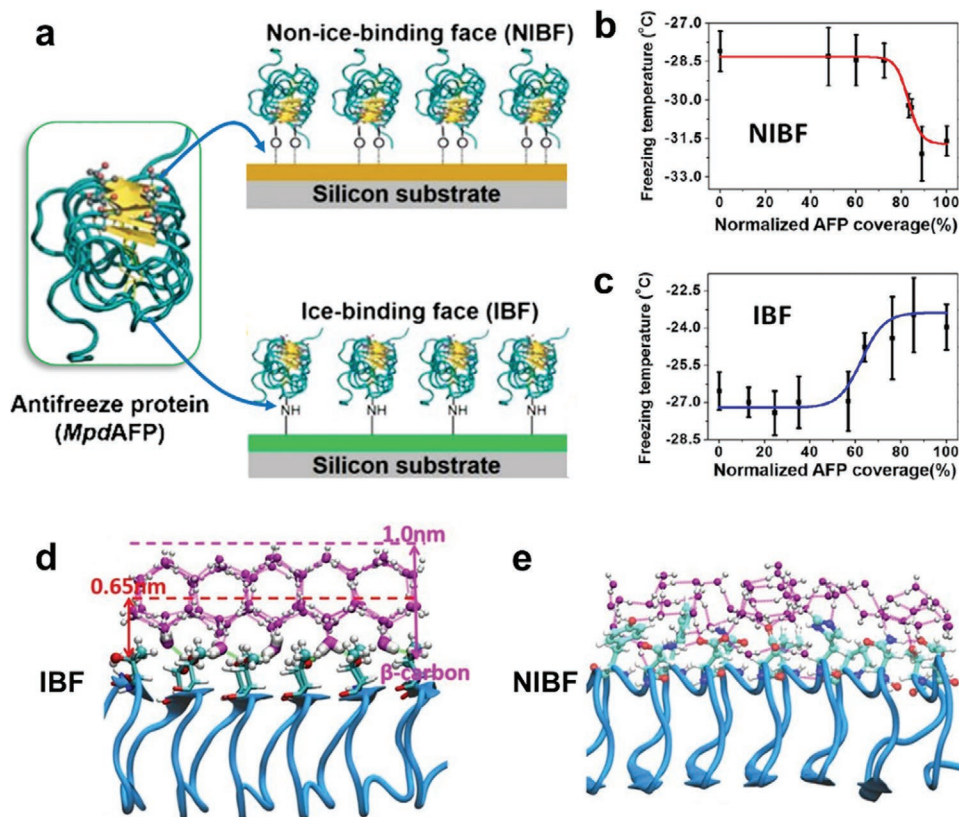
Figure 3. Janus effect of antifreeze proteins on ice nucleation. a) Schemes illustrate the selective grafting of the nonice-binding face (NIBF) and ice-binding face (IBF) of an AFP on solid surface. b,c) Ice nucleation temperature of water droplet (0.1 µL) on the b) NIBF and c) IBF surfaces with different grafting density. d,e) Molecular dynamics (MD) simulation analysis to show molecular level mechanism of AFPs in tuning ice nucleation. a–e) Reproduced with permission.[7e] Copyright 2016, PNAS.

3. Ice Growth Patterns on Solid Surface

The final state of ice on surface is usually determined by the growth of ice crystals in specific situations. The natural morphology of ice crystals can be influenced by the interaction between external macroscopic forces and microscopic interfacial behavior.[40] The ice frozen on the window tends to spread along the surface and finally form an ice layer strongly attached. Snow deposited on the surface transits to ice block when the temperature and humidity change. In addition, frost morphologies exhibit a significant dependence on the supercooling degree and relative humidity.[41] In conditions which ice nucleation is inevitable, the growth or evolution of ice crystal determines the ice-adhesion to surfaces. Studies on the ice growth on solid surfaces in nanoscale have been studied for tens of years.[31b,42] However, a correlation between various factors induced microscopic water structures and the macroscopic patterns of ice crystals supported by solid surfaces has rarely been investigated.

Recently, Liu et al. found that ice crystals exhibit distinct growth modes on surfaces with different wetting properties.[12c] They found that ice undergoes off-surface growth (OSG) mode on a hydrophobic surface (contact angle θ is 107.3°) and along surface growth (ASG) mode on a hydrophilic surface (contact angle θ is 14.5°) (**Figure** 4a,b). The growth mode transition was observed when the wetting property of solid surfaces changes. On the smooth surface, the ASG-to-OSG transition occurs when the

contact angle of water becomes larger than 32.5° ± 1.9° (Figure 4c). This transition also happens on the anodic aluminum oxide (AAO) surfaces independent of morphologies (Figure 4c). Through spatially introducing AgI as ice nucleation agent on superhydrophobic surface, the ice formation was controlled. The OSG growth mode of ice leads to tiny contact area to the surface, as a result, the ice can be easily removed from surface by breeze (5 m s⁻¹) (Figure 4d).

Ice propagation is another factor causing ice deposition on the solid surface.[43] They studied the ice propagation behavior on polyelectrolyte multilayer (PEM) surfaces (Figure 4e). The ice propagation is strongly dependent on the amount of water in the outermost layer of PEMs. The ice propagation rate can be tuned by up to three orders of magnitude by changing the polyelectrolyte pairs, counter ions of the polymer layer, or the salt concentration (Figure 4f). By introducing polymer brushes with specific patterns, the high-speed propagation leads to a spatial formation of ice on the surface.[44] With this method, the ice coverage on the surface can be significantly decreased.

4. Anti-Icing or De-icing Strategies

4.1. Reducing Ice Adhesion by Liquid Lubricants

For surfaces which have been deposited with ice, reducing ice adhesion becomes an effective means to decrease the de-icing
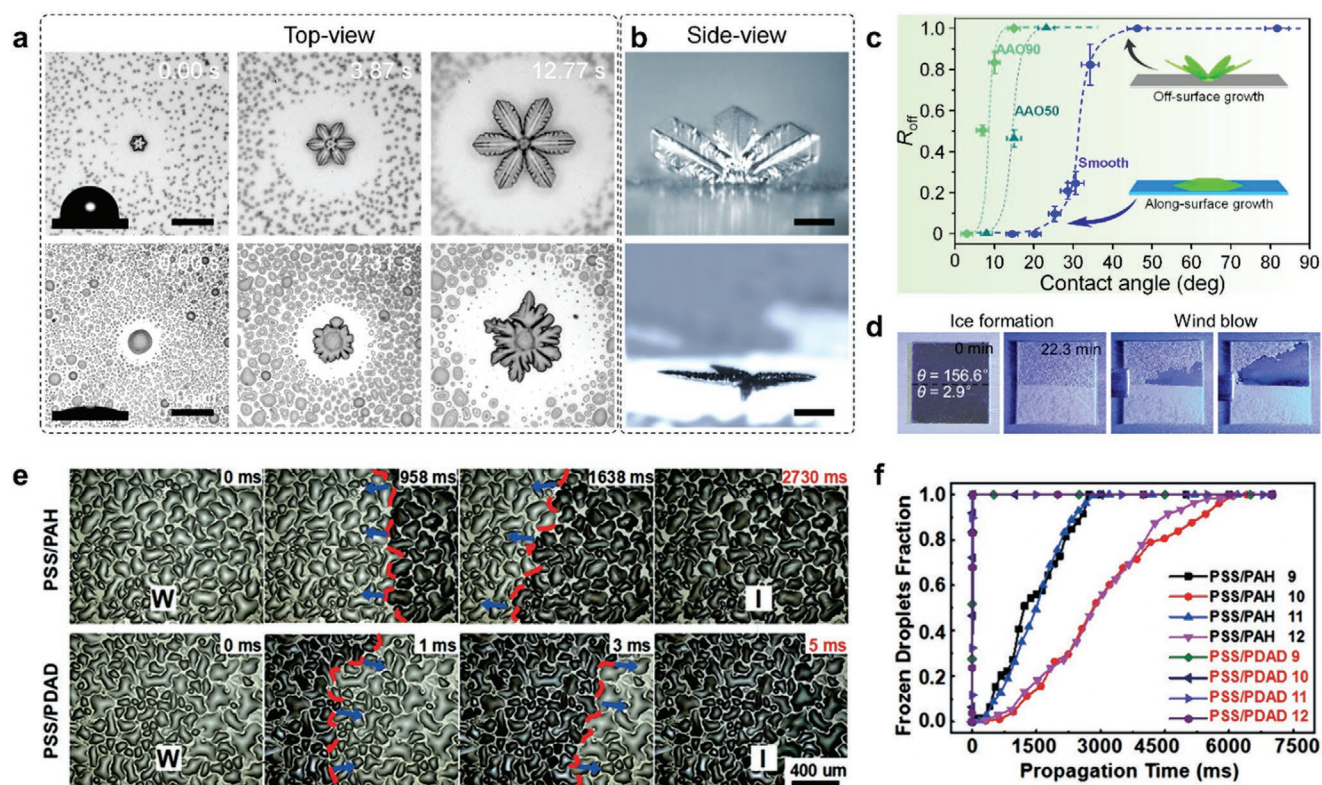
Figure 4. Ice growth and propagation on solid surface. a) Distinct ice growth on hydrophobic (upper) and hydrophilic (lower) surface. Scale bar: 30 μm. b) A side-view snapshot that shows the morphology of the ice on the hydrophobic and hydrophilic surface. c) The ASG-to-OSG transition at a critical contact angle. d) Design of an anti-icing surface. a–d) Reproduced with permission.[12c] Copyright 2016, PNAS. e) The optical microscopic images of ice propagation on the PSS (poly(sodium-p-styrene sulfonate))/PAH (poly(allylamine hydrochloride)) (n = 9) (upper) and PSS/PDAD (poly(diallyldimethylammonium chloride)) (n = 9) (lower) for various times. f) The fraction of frozen condensed water droplets on the PEM surfaces. e,f) Reproduced with permission.[43] Copyright 2017, Wiley-VCH.

difficulties. Inspired by the lubricating effect of the quasi-liquid in ice skating, Chen et al. reported to introduce a self-lubricated aqueous layer on surfaces to reduce ice adhesion (**Figure 5**a).[45] Dopamine and hyaluronic acid are employed to fabricate the thin layer of hydrogel on surface. After adsorbing water, the cross-linked hyaluronic acid begins to swell and forms an aqueous lubricating layer (Figure 5a,b). After treating different surfaces including metals and polymers with such coating, the ice adhesion strength on the surface was found to be more than one order of magnitude lower than the untreated surfaces (Figure 5c,d). To enhance the robustness of the surface, Chen et al. proposed to use the solid microstructure as a protection of the coating. They filled the hydrophilic and hygroscopic polymers (poly(acrylic acid)) inside the micropores on the surface, and the surface presents outstanding stability in repeatedly de-icing procedures with a low ice adhesion (Figure 5e).[46]

Hydrophilic anti-icing surfaces could also be prepared by being infiltrated with amphiphilic lubricants on surfaces. Yu et al. fabricated an amphiphilic organogels (AmOG-2) which is infiltrated with amphiphilic lubricant PEO-PDMS-PEO (M_w = 9200, PEO (poly(ethylene oxide))/PDMS (poly(dimethylsiloxane)) = 15.0%) (AmO-2).[47] When exposed to water, the hydrophilic segments of the amphiphilic lubricant combines with water molecules through hydrogen bond to form nonfreezable bond water. This decreases the freezing

point of water and delays the formation of ice crystals on the surface. In addition, amphiphilic lubricants could motivate the formation of a self-lubricating aqueous layer by absorbing water molecules from air to decrease the ice adhesion.

Wong et al. reported a slippery liquid-infused porous surface(s) (SLIPS) with exceptional liquid- and ice-repellency.[48] Inspired by Nepenthes pitcher plants,[49] low-surface-tension perfluorinated liquids were infused into nanoposts functionalized arrays with a low-surface energy fluorinated silane, or a random network of Teflon nanofibers (Figure 5f,g).[50] SLIPS could maintain low contact angle hysteresis (<2.5°) and quickly restore liquid-repellency after physical damages. The high mobility of the liquid lubricant leads to ultra-low ice adhesion to surfaces, thus ice blocks show good mobility on a tilted SLIPS (Figure 5h). Introducing the SLIPS with other functionalities could enhance its anti-icing property in reducing the freezing temperature, ice adhesion strength, and even the cost. Irajizad et al. have reported a new magnetic SLIPS which performs icephobic properties with an ice formation temperature of −34 °C, long delay time in ice formation, and extremely low ice adhesion strength.[51] The magnetic field locks the ferrofluid in place, and thus the magnetic SLIPS can withstand extreme shear stresses. The anti-icing test on the magnetic SLIPS shows that the ice adhesion strength on such surface (≈2 Pa) is about five orders of magnitude lower than the reported values for

**ADVANCED
SCIENCE NEWS**

www.advancedsciencenews.com

**ADVANCED
MATERIALS
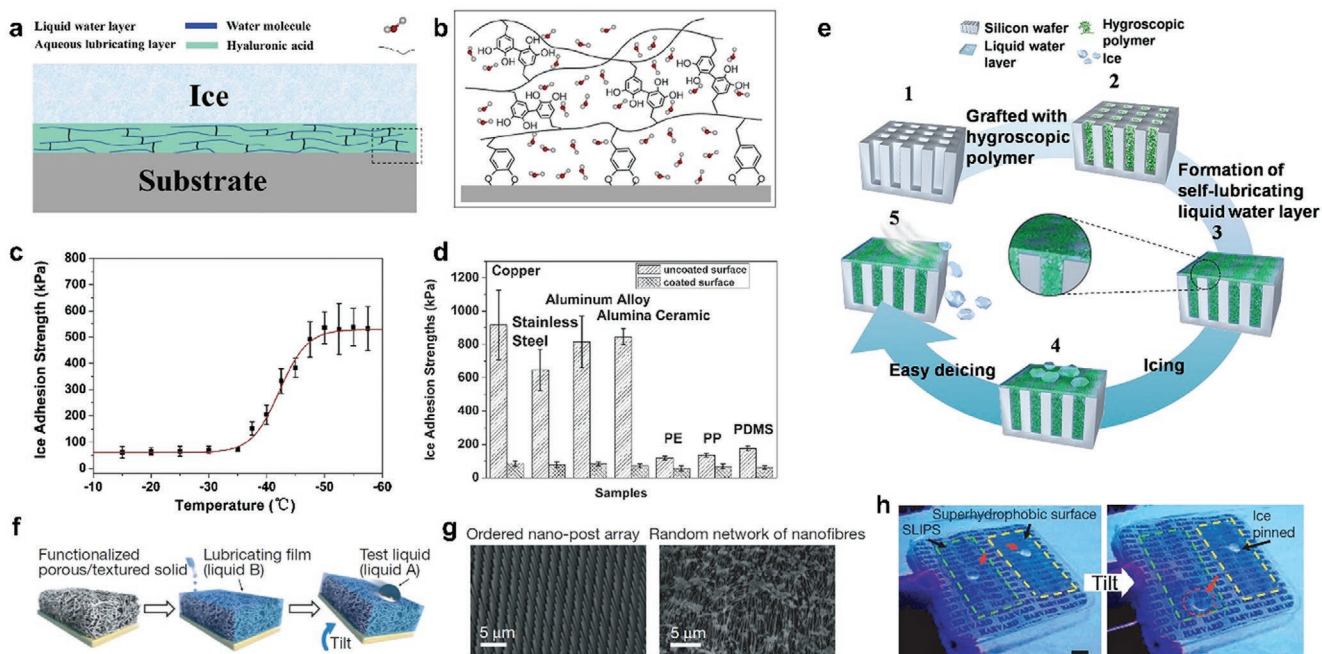INTERFACES**

www.advmatinterfaces.de

Figure 5. Lubricated surfaced with low ice adhesion. a) Schematic illustration of the anti-icing coating with aqueous lubricating layer based on hyaluronic acid and dopamine. b) Scheme shows the chemical composition of the aqueous lubricating layer. c) Ice adhesion on the aqueous lubricating layer at different temperatures. d) Ice adhesion on various surfaces. a–d) Reproduced with permission.[45] Copyright 2014, Wiley-VCH. e) Scheme shows the repeatedly de-icing process on the aqueous lubricating layer with microstructures. Reproduced with permission.[46] Copyright 2013, American Chemical Society. f,g) Schematics show the fabrication of a SLIPS by infiltrating a functionalized porous/textured solid with a low-surface energy, chemically inert liquid. h) Ice mobiles on a SLIPS (highlighted in green) compared to the strong adhesion to an epoxy-resin-based nanostructured superhydrophobic surface (highlighted in yellow). f–h) Reproduced with permission.[48] Copyright 2011, Springer Nature.

icephobic surfaces.[1d] Ice frozen from a water droplet exhibits a good mobility on different substrates with magnetic SLIPS.

4.2. Reducing Ice Adhesion by Low Toughness Surfaces

Recently, a new finding by Golovin et al. illustrated that the force required to remove adhered ice on large areas (few cm^2 or greater) of low-interfacial toughness (LIT) materials was both low and independent of the area.[52] They found that the force (per unit width) required to detach the ice ($\tilde{F}_{ice}$) increases proportionally to L (L: the length of the interface) when L was at a small value, while once the length of ice is beyond the transition length L_c, interfacial toughness Γ could affect the ice adhesion a lot (**Figure 6**a,b). The corresponding asymptotic force with L_c, $\tilde{F}_{ice}^{cr}$, is used to determine the interfacial toughness, Γ, according to $\Gamma = (\tilde{F}_{ice}^{cr})^2/2E_{ice}h$,[53] where E_{ice} is the modulus of ice with thickness of h. When at short length, though the toughness of polypropylene is lower than that of silicon B (a kind of PDMS from Mold Max STROKE of Smooth-On Inc. mixed in a 10:1 base:crosslinker ratio), silicon B exhibits a lower ice adhesion strength than the polypropylene. However, the $\tilde{F}_{ice}$ continually increases with the length of silicone B, as a result, the ice is removed more easily from polypropylene ($\Gamma = 1.9$ J m^{-2}) than from the silicone B ($\Gamma > 9$ J m^{-2}) when $L > 50$ cm. The apparent ice adhesion strength (τ_{ice}) on polypropylene ($\tau_{ice} \approx 12$ kPa) was less than the half-value of that on the icephobic PDMS ($\tau_{ice} \approx 29$ kPa) when $L = 100$ cm (Figure 6b).

The LIT surfaces were prepared by coating a lubricated layer with the thickness of 1–2 μm on 1.2 m long aluminum beams and this coating can be composed of PDMS and silicone oil (LIT PDMS, $\Gamma = 0.12 \pm 0.03$ J m^{-2}), polyvinyl chloride (PVC) and medium-chain triglyceride oil (LIT PVC, $\Gamma = 0.27 \pm 0.07$ J m^{-2}), or polystyrene and diisodecyl adipate (LIT PS, $\Gamma = 0.43 \pm 0.08$ J m^{-2}). In Figure 6c, we can see that the $\tilde{F}_{ice}$ on aluminum beams coated with LIT PVC and LIT PDMS stop increasing when $L > L_c$ ($\tilde{F}_{ice}^{cr} = 52 \pm 7$ N cm^{-1} for LIT PVC, $\tilde{F}_{ice}^{cr} = 35 \pm 4$ N cm^{-1} for LIT PDMS). Upon flexing the surface, ice is fractured cleanly from the LIT PDMS at a low deflection of 2.4 cm from the center of the beam (Figure 6d). In contrast, both the uncoated and icephobic-coated beams displayed limited signs of ice detachment even at an extreme deflection of ≈35 cm. Therefore, the LIT coatings are more meaningful in de-icing of large area surface such as an airplane via wing tip deflection.

4.3. Anti-Icing Superhydrophobic Surfaces

The superhydrophobic surface is a kind of liquid-repellent surface on which the apparent contact angles of water are larger than 150°. The low-adhesion leads to the high motilies of water drops on the superhydrophobic surfaces, e.g., coalescence of condensed droplets induced jumping, bouncing followed drop impingement, rolling, etc.[9a,17b,54] Benefit from these characteristics, superhydrophobic surfaces display significant advantages of reducing water accretion before ice formation.
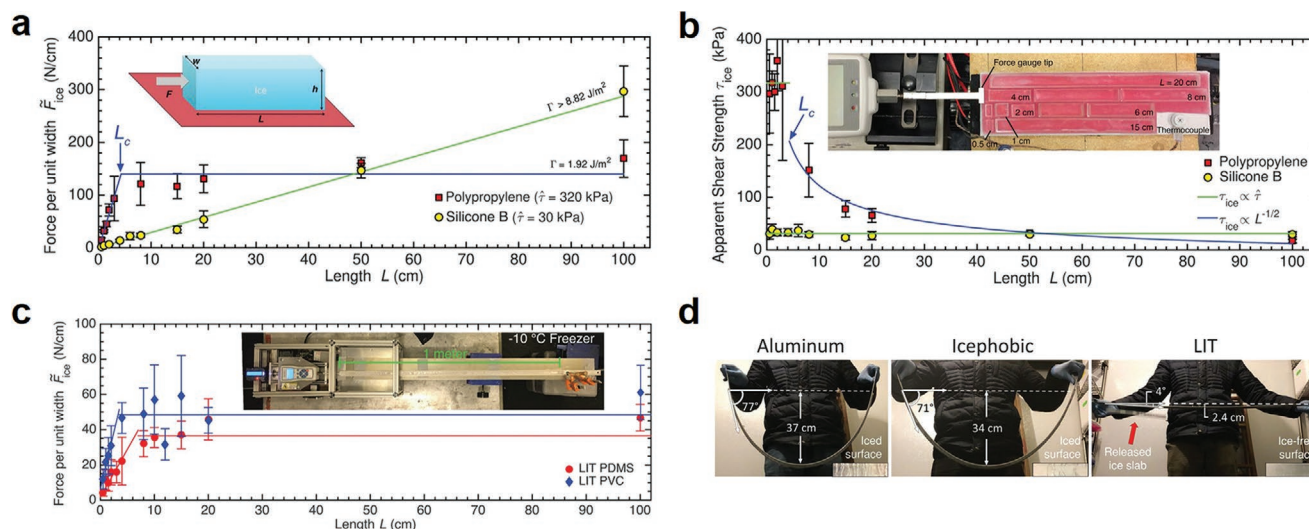
2100327 (7 of 12)

Figure 6. Low toughness surface with low ice adhesion. a) The force per unit width required to detach ice ($\tilde{F}_{ice}$) from silicone B and polypropylene as a function of interfacial length (L). The inset shows the method to measure $\tilde{F}_{ice}$. b) The apparent shear strength τ_{ice} of ice on the silicone B and the polypropylene as functions of L. The inset shows the setup used to test τ_{ice} of 11 pieces of ice with different lengths. c) The $\tilde{F}_{ice}$ on the LIT PDMS and LIT PVC surfaces as functions of L at −10 °C. The inset shows the measurement of $\tilde{F}_{ice}$ with an interfacial length of 1 m. d) Ice fractured from the uncoated and icephobic aluminum surface and LIT-coated specimen undergoing off-center load flex tests at −20 °C. a–d) Reproduced with permission.[52] Copyright 2019, AAAS.

Hou et al. fabricated superhydrophobic surface with biphilic topography by introducing patterned high-contrast wettability.[55] The biphilic surface consists of micropillar arrays with hydrophilic tops surrounded by superhydrophobic nanograsses. They found that the biphilic surface exhibits better suppression on ice nucleation than the hydrophobic surface and homogenous superhydrophobic surface (**Figure 7**a). The supercooled droplets on the hydrophobic surface tend to freeze when their radii is ≈50 μm at substrate temperature of 267.75 ± 0.15 K (Figure 7b). By contrast, the droplet freezing radii on the superhydrophobic (≈70 μm) and biphilic (≈100 μm) surfaces are, respectively, 1.4 and 2 times of that on the hydrophobic surface. Attributed to the spatial hydrophilic micropillar arrays, the condensation sites of water are spatially controlled. As a result, droplets tend to depart from the biphilic surface at a low level of droplet size, which results in less water deposits on the surface. As a result, ice nucleation on the biphilic surface is effectively suppressed. Inspired by this work, decreasing the condensate droplet size can improve the anti-icing activity of the surface. Another surface to reduce condensate droplet size was reported by Liu et al. (Figure 7c),[56] in which they effectively reduced the size of the condensate water droplet by introducing anisotropic microstructures on superhydrophobic surface, accompanying which the periodic adhesion gradients of water are established on the surface. Steered by the microscale adhesion gradient, the jumping direction of coalesced droplets is defined. With this effect, the departure efficiency of water is significantly enhanced by 100% compared to the homogenous superhydrophobic surface.

A drop striking a superhydrophobic surface will spread out to a maximum diameter and then recoil until to rebounce and leave the surface. The amount of time that the drop is in contact with the solid—the "contact time"—depends on the inertia and capillarity of the drop, internal dissipation, and surface–liquid interactions.[17b,57] Impacting of supercooled water drops on the surface might cause freezing and ice deposition. Timely detachment of water drops from the surface contributes to reducing the induction time for ice nucleation. Various superhydrophobic surfaces have been designed to reduce the contact time.[17a,58] Varanasi et al. reduced the contact time by using superhydrophobic surfaces with a morphology that redistributes the liquid mass and thereby alters the drop hydrodynamics (Figure 7d). When drops impact on the surface, they are cut to pieces at the largest spreading length. With less masses, the broken drops have faster dynamics and detach from the surface rapidly. In addition, Wang et al. introduced lattices of submillimeter-scale posts decorated with nanostructures on the surface (Figure 7e)[58a] The drops spread when impacting on the surface and then detach from such surface in a flattened, pancake shape. As the drops leave the surface before recoiling process, the contact time is significantly reduced. Therefore, the subcooling drops can detach rapidly from the surface before icing happens.

4.4. Others

Functional superhydrophobic surfaces with photothermal or electrothermal properties also exhibit their unique advantages in anti-icing.[59] Upon illumination under sun or powering, these photo/electro-thermal surfaces can melt the accumulated ice easily and then immediately remove the melted water by the superhydrophobicity. Wu et al. reported a candle soot base superhydrophobic surface on which the surface temperature increases when illuminated by sun light (Figure 7f).[59a] This light-induced heating raises the surface temperature above 0 °C, which leads to the melting of ice at the interface and finally to the detachment from the surface. With no external force required, this method of autonomous de-icing will have very promising applications.
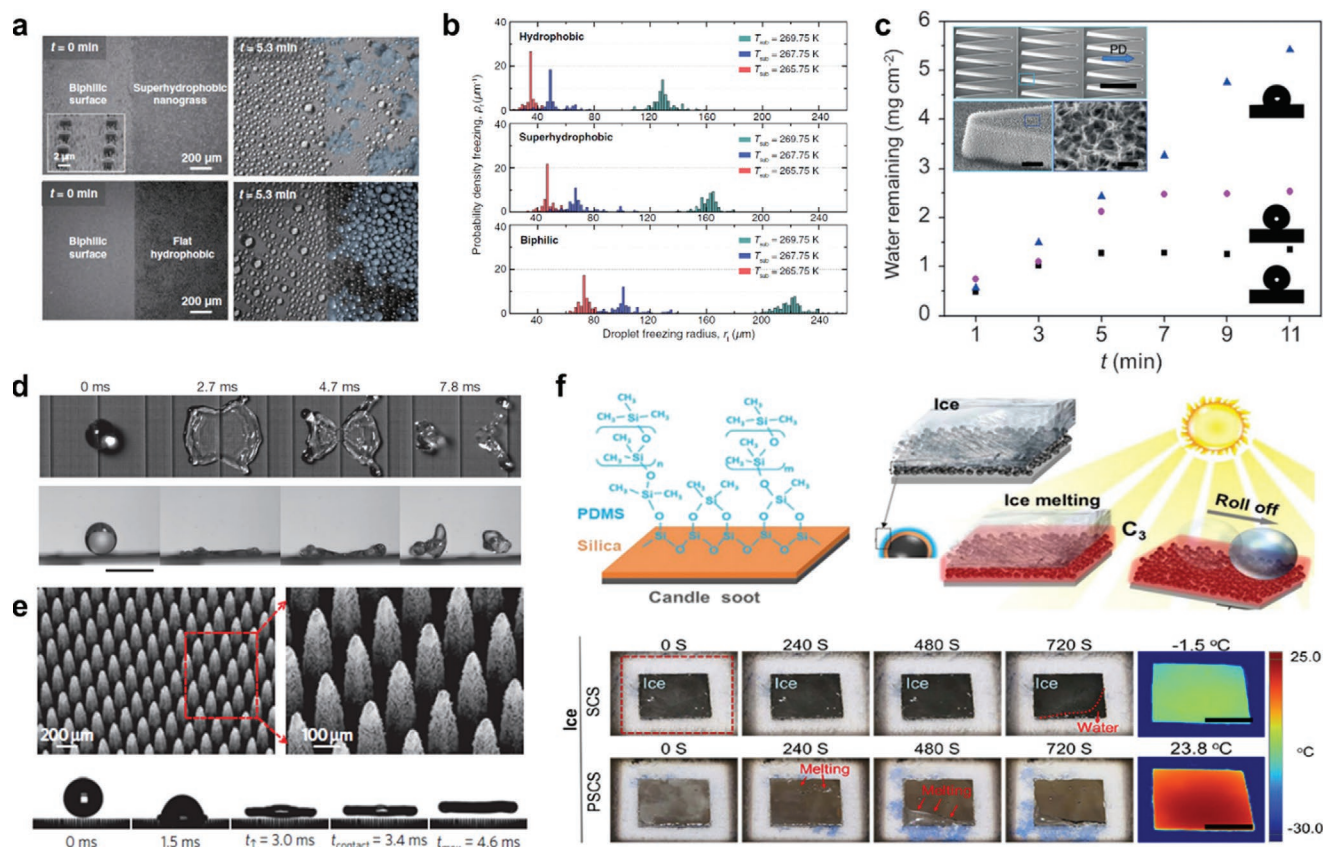
**ADVANCED
SCIENCE NEWS**

www.advancedsciencenews.com

**ADVANCED
MATERIALS
INTERFACES**

www.advmatinterfaces.de

Figure 7. Superhydrophobic surface suppressing ice formation. a) Comparison of ice nucleation activity of the hydrophobic surface, homogenous superhydrophobic surface, and superhydrophobic surface with biphilic topography. Temperature: 267.75 ± 0.15 K. b) Probability density freezing distribution as functions of droplet radii on the hydrophobic surface, homogenous superhydrophobic surface, and superhydrophobic surface with biphilic topography. a,b) Reproduced with permission.[55] Copyright 2018, American Physical Society. c) The removal efficiency of condensate water on hydrophobic surface, homogenous superhydrophobic surface, and superhydrophobic surface with anisotropic microstructures. Inset shows the morphology of the anisotropic surface. Reproduced with permission.[56] Copyright 2016, Wiley-VCH. d) Droplet impacts on the superhydrophobic surface with the macroscopic structure. Scale bar: 4 mm. Reproduced with permission.[17a] Copyright 2013, Springer Nature. e) Pancake bouncing of water drops on a superhydrophobic surface with a square lattice of tapered posts. Reproduced with permission.[58a] Copyright 2014, Springer Nature. f) A superhydrophobic, photothermal, and icephobic surface based on candle soot. Covered ice on the surface melts under illumination of sunlight. Reproduced with permission.[59a] Copyright 2020, PNAS.

5. Conclusion

Researches on anti-icing surfaces have been conducted for decades. In this review, we summarized both theoretical and experimental progresses of heterogenous ice nucleation on solid surfaces. Based on the understanding of the ice nucleation, various surfaces have been designed to achieve suppression of ice nucleation to a certain extent in specific circumstances. The shortcoming is that most of the current surfaces resist ice nucleation only for a certain period. In the end, ice will form on the surface. In addition, usually in air condition, the dust, air flow, humidity, etc., existing in air might also cause nucleation. In order to prepare a perfect ice-free surface, besides extending delay time of ice nucleation factors from air must be taken into account.

By intentionally regulating the ice growth process, the final state of the ice on solid surface can be controlled. As introduced in Figure 4, the change of ice growth mode on hydrophobic or superhydrophobic surfaces significantly minimizes the contact area of ice and surface. An effective antifrost surface was designed according to this method. Besides wetting properties,

the factors such as electric field, charges, chemical composition, and crystal lattice can all have influences on the growth of ice crystals on the solid surfaces. This will be significantly meaningful for designing effective de-icing strategies in the future.

Till now, the most famous surfaces with low ice adhesion can be summarized to hydrophilic self-lubricated surface, oil refused lubricated surface, and superhydrophobic surfaces. The ice adhesion strength on some of these surfaces has been reduced to a very low level, $\tau_{ice} < 10$ kPa. However, aiming for long-term utility in practice, the robustness of the surfaces withstanding abrasion, degradation, or corrosion deserves high attentions. The manufacture complexity, cost, and environmental friendly should also be the general considerations.

Conflict of Interest

The authors declare no conflict of interest.

Keywords

[1] a) X. Yao, Y. Song, L. Jiang, *Adv. Mater.* **2011**, *23*, 719; b) J. Xiao, S. Chaudhuri, *Langmuir* **2012**, *28*, 4434; c) Q. Li, Z. Guo, *J. Mater. Chem. A* **2018**, *6*, 13549; d) J. Lv, Y. Song, L. Jiang, J. Wang, *ACS Nano* **2014**, *8*, 3152.

[2] a) A. P. Broeren, S. Lee, C. Clark, *J. Aircr.* **2016**, *53*, 451; b) O. Parent, A. Ilinca, *Cold Reg. Sci. Technol.* **2011**, *65*, 88.

[3] A. Emerym, B. Siegel, *Heat and Mass Transfer in Fires: Presented at Aiaa/Asme Thermophysics and Heat Transfer Conference*, Vol. *1*, American Society of Mechanical Engineers Heat Transfer Division, Seattle, Washington **1990**.

[4] a) Z. He, K. Liu, J. Wang, *Acc. Chem. Res.* **2018**, *51*, 1082; b) M. J. Kreder, J. Alvarenga, P. Kim, J. Aizenberg, *Nat. Rev. Mater.* **2016**, *1*, 15003.

[5] a) J. Li, Y. Luo, J. Zhu, H. Li, X. Gao, *ACS Appl. Mater. Interfaces* **2015**, *7*, 26391; b) J. Laforte, M. Allaire, J. Laflamme, *Atmos. Res.* **1998**, *46*, 143; c) L. B. Boinovich, A. M. Emelyanenko, *Mendeleev Commun.* **2013**, *1*, 3.

[6] Z. Zhang, X. Y. Liu, *Chem. Soc. Rev.* **2018**, *47*, 7116.

[7] a) R. Chatterjee, D. Beysens, S. Anand, *Adv. Mater.* **2019**, *31*, 1807812; b) P. Guo, Y. Zheng, M. Wen, C. Song, Y. Lin, L. Jiang, *Adv. Mater.* **2012**, *24*, 2642; c) H. Yang, C. Ma, K. Li, K. Liu, M. Loznik, R. Teeuwen, J. C. van Hest, X. Zhou, A. Herrmann, J. Wang, *Adv. Mater.* **2016**, *28*, 5008; d) G. Bai, D. Gao, Z. Liu, X. Zhou, J. Wang, *Nature* **2019**, *576*, 437; e) K. Liu, C. Wang, J. Ma, G. Shi, X. Yao, H. Fang, Y. Song, J. Wang, *Proc. Natl. Acad. Sci. U. S. A.* **2016**, *113*, 14739.

[8] a) T. M. Schutzius, S. Jung, T. Maitra, G. Graeber, M. Kohme, D. Poulikakos, *Nature* **2015**, *527*, 82; b) P. Kant, R. B. J. Koldeweij, K. Harth, M. A. J. van Limbeek, D. Lohse, *Proc. Natl. Acad. Sci. U. S. A.* **2020**, *117*, 2788.

[9] a) Q. Zhang, M. He, J. Chen, J. Wang, Y. Song, L. Jiang, *Chem. Commun.* **2013**, *49*, 4516; b) J. B. Boreyko, C. P. Collier, *ACS Nano* **2013**, *7*, 1618; c) L. Mishchenko, J. Aizenberg, B. D. Hatton, *Adv. Funct. Mater.* **2013**, *23*, 4577; d) X. Chen, R. Ma, H. Zhou, X. Zhou, L. Che, S. Yao, Z. Wang, *Sci. Rep.* **2013**, *3*, 2515.

[10] a) G. Bai, Z. Song, H. Geng, D. Gao, K. Liu, S. Wu, W. Rao, L. Guo, J. Wang, *Adv. Mater.* **2017**, *29*, 1606843; b) H. Geng, X. Liu, G. Shi, G. Bai, J. Ma, J. Chen, Z. Wu, Y. Song, H. Fang, J. Wang, *Angew. Chem., Int. Ed.* **2017**, *129*, 1017.

[11] a) L. Lupi, A. Hudait, B. Peters, M. Grunwald, R. Gotchy Mullen, A. H. Nguyen, V. Molinero, *Nature* **2017**, *551*, 218; b) E. B. Moore, V. Molinero, *Nature* **2011**, *479*, 506.

[12] a) B. Xue, L. S. Zhao, X. H. Qing, M. Qin, J. C. Lai, W. M. Huang, H. Lei, J. J. Wang, W. Wang, Y. Li, Y. Cao, *ACS Macro Lett.* **2019**, *8*, 1383; b) H. Y. Geng, B. W. Yao, J. J. Zhou, K. Liu, G. Y. Bai, W. B. Li,

[13] a) S. W. Wu, L. H. Li, H. Xue, K. Liu, Q. R. Fan, G. Y. Bai, J. J. Wang, *ACS Nano* **2017**, *11*, 9898; b) S. W. Wu, C. Q. Zhu, Z. Y. He, H. Xue, Q. R. Fan, Y. L. Song, J. S. Francisco, X. C. Zeng, J. J. Wang, *Nat. Commun.* **2017**, *8*, 15154.

[14] a) D. H. Veeregowda, A. Kolbe, H. C. van der Mei, H. J. Busscher, A. Herrmann, P. K. Sharma, *Adv. Mater.* **2013**, *25*, 3426; b) D. Ehre, E. Lavert, M. Lahav, I. Lubomirsky, *Science* **2010**, *327*, 672; c) F. K. Odencrantz, R. W. Buecher, *Science* **1967**, *158*, 256.

[15] X. Sun, K. Rykaczewski, *ACS Nano* **2017**, *11*, 906.

[16] L. Wang, Q. Gong, S. Zhan, L. Jiang, Y. Zheng, *Adv. Mater.* **2016**, *28*, 7729.

[17] a) J. C. Bird, R. Dhiman, H.-M. Kwon, K. K. Varanasi, *Nature* **2013**, *503*, 385; b) D. Richard, C. Clanet, D. Quéré, *Nature* **2002**, *417*, 811; c) L. Wang, R. Wang, J. Wang, T.-S. Wong, *Sci. Adv.* **2020**, *6*, eabb2307.

[18] a) X. Yan, L. Zhang, S. Sett, L. Feng, C. Zhao, Z. Huang, H. Vahabi, A. K. Kota, F. Chen, N. Miljkovic, *ACS Nano* **2019**, *13*, 1309; b) C.-H. Chen, K. M. Wisdom, J. A. Watson, X. Qu, F. Liu, G. S. Watson, *Proc. Natl. Acad. Sci. U. S. A.* **2013**, *110*, 7992; c) J. B. Boreyko, R. R. Hansen, K. R. Murphy, S. Nath, S. T. Retterer, C. P. Collier, *Sci. Rep.* **2016**, *6*, 19131.

[19] T.-S. Wong, S. H. Kang, S. K. Y. Tang, E. J. Smythe, B. D. Hatton, A. Grinthal, J. Aizenberg, *Nature* **2011**, *477*, 443.

[20] J. D. Atkinson, B. J. Murray, D. O'Sullivan, *J. Phys. Chem. A* **2016**, *120*, 6513.

[21] a) J. M. Campbell, F. C. Meldrum, H. K. Christenson, *J. Phys. Chem. C* **2015**, *119*, 1164; b) J. D. Atkinson, B. J. Murray, M. T. Woodhouse, T. F. Whale, K. J. Baustian, K. S. Carslaw, S. Dobbie, D. O'Sullivan, T. L. Malkin, *Nature* **2013**, *498*, 355.

[22] a) S. Jin, Y. Liu, M. Deiseroth, J. Liu, E. H. G. Backus, H. Li, H. Xue, L. Zhao, X. C. Zeng, M. Bonn, J. Wang, *J. Am. Chem. Soc.* **2020**, *142*, 17956; b) A. Kiselev, F. Bachmann, P. Pedevilla, S. J. Cox, A. Michaelides, D. Gerthsen, T. Leisner, *Science* **2017**, *355*, 367; c) M. Gavish, R. Popovitz-Biro, M. Lahav, L. Leiserowitz, *Science* **1990**, *250*, 973; d) Z. Zhang, Y. Ying, M. Xu, C. Zhang, Z. Rao, S. Ke, Y. Zhou, H. Huang, L. Fei, *Nano Lett.* **2020**, *20*, 8112.

[23] H. Xue, Y. Lu, H. Geng, B. Dong, S. Wu, Q. Fan, Z. Zhang, X. Li, X. Zhou, J. Wang, *J. Phys. Chem. Lett.* **2019**, *10*, 2458.

[24] a) R. O. David, C. Marcolli, J. Fahrni, Y. Qiu, Y. A. Perez Sirkin, V. Molinero, F. Mahrt, D. Brühwiler, U. Lohmann, Z. A. Kanji, *Proc. Natl. Acad. Sci. U. S. A.* **2019**, *116*, 8184; b) J. M. Campbell, F. C. Meldrum, H. K. Christenson, *Proc. Natl. Acad. Sci. U. S. A.* **2017**, *114*, 810.

[25] A. Belitzky, E. Mishuk, D. Ehre, M. Lahav, I. Lubomirsky, *J. Phys. Chem. Lett.* **2015**, *7*, 43.

[26] Z. He, W. J. Xie, Z. Liu, G. Liu, Z. Wang, Y. Q. Gao, J. Wang, *Sci. Adv.* **2016**, *2*, e1600345.

[27] a) Z. A. Kanji, A. Welti, C. Chou, O. Stetzer, U. Lohmann, *Atmos. Chem. Phys.* **2013**, *13*, 9097; b) N. S. Umo, R. Wagner, R. Ullrich, A. Kiselev, H. Saathoff, P. G. Weidler, D. J. Cziczo, T. Leisner, O. Möhler, *Atmos. Chem. Phys.* **2019**, *19*, 8783; c) H.-M. Hung, A. Malinowski, S. T. Martin, *J. Phys. Chem. A* **2002**, *106*, 293; d) C. R. Hoyle, V. Pinti, A. Welti, B. Zobrist, C. Marcolli, B. Luo, Á. Höskuldsson, H. B. Mattsson, O. Stetzer, T. Thorsteinsson, G. Larsen, T. Peter, *Atmos. Chem. Phys.* **2011**, *11*, 9911; e) R. Iannone, D. I. Chernoff, A. Pringle, S. T. Martin, A. K. Bertram, *Atmos. Chem. Phys.* **2011**, *11*, 1191.

[28] a) N. H. Fletcher, *J. Chem. Phys.* **1958**, *29*, 572; b) A. Welti, F. Lüönd, O. Stetzer, U. Lohmann, *Atmos. Chem. Phys.* **2009**, *9*, 6705; c) C. Hoose, O. Möhler, *Atmos. Chem. Phys.* **2012**, *12*, 9817; d) Y.-C. Liou, A. Tocilj, P. L. Davies, Z. Jia, *Nature* **2000**, *406*, 322; e) C. P. Garnham, R. L. Campbell, V. K. Walker, P. L. Davies, *BMC Struct. Biol.* **2011**, *11*, 36.

**ADVANCED
SCIENCE NEWS**

www.advancedsciencenews.com

**ADVANCED
MATERIALS
INTERFACES**

www.advmatinterfaces.de

[29] G. Vali, P. J. DeMott, O. Möhler, T. F. Whale, *Atmos. Chem. Phys.* **2015**, *15*, 10263.

[30] T. Häusler, P. Gebhardt, D. Iglesias, C. Rameshan, S. Marchesan, D. Eder, H. Grothe, *J. Phys. Chem. C* **2018**, *122*, 8182.

[31] a) H. Geng, X. Liu, G. Shi, G. Bai, J. Ma, J. Chen, Z. Wu, Y. Song, H. Fang, J. Wang, *Angew. Chem., Int. Ed.* **2017**, *56*, 997; b) Y. Zheng, C. Su, J. Lu, K. P. Loh, *Angew. Chem., Int. Ed.* **2013**, *52*, 8708.

[32] G. Y. Bai, D. Gao, Z. Liu, X. Zhou, J. J. Wang, *Nature* **2019**, *576*, 437.

[33] M. Joghataei, F. Ostovari, S. Atabakhsh, N. Tobeiha, *Sci. Rep.* **2020**, *10*, 9723.

[34] a) X. Chen, T. Yang, S. Kataoka, P. S. Cremer, *J. Am. Chem. Soc.* **2007**, *129*, 12272; b) S. Nihonyanagi, S. Yamaguchi, T. Tahara, *J. Am. Chem. Soc.* **2014**, *136*, 6155; c) T. Koop, B. Luo, A. Tsias, T. Peter, *Nature* **2000**, *406*, 611.

[35] a) J. Drzymala, Z. Sadowski, L. Holysz, E. Chibowski, *J. Colloid Interface Sci.* **1999**, *220*, 229; b) H. Watanabe, T. Otsuka, M. Harada, T. Okada, *J. Phys. Chem. C* **2014**, *118*, 15723.

[36] L. Eickhoff, K. Dreischmeier, A. Zipori, V. Sirotinskaya, C. Adar, N. Reicher, I. Braslavsky, Y. Rudich, T. Koop, *J. Phys. Chem. Lett.* **2019**, *10*, 966.

[37] K. Meister, S. Lotze, L. L. C. Olijve, A. L. DeVries, J. G. Duman, I. K. Voets, H. J. Bakker, *J. Phys. Chem. Lett.* **2015**, *6*, 1162.

[38] J. A. Raymond, A. L. DeVries, *Proc. Natl. Acad. Sci. U. S. A.* **1977**, *74*, 2589.

[39] a) A. Abdelmonem, E. H. G. Backus, N. Hoffmann, M. A. Sánchez, J. D. Cyran, A. Kiselev, M. Bonn, *Atmos. Chem. Phys.* **2017**, *17*, 7827; b) B. Glatz, S. Sarupria, *J. Chem. Phys.* **2016**, *145*, 211924; c) E. Anim-Danso, Y. Zhang, A. Dhinojwala, *J. Phys. Chem. C* **2016**, *120*, 3741.

[40] E. Ben-Jacob, P. Garik, *Nature* **1990**, *343*, 523.

[41] a) K. K. Varanasi, T. Deng, J. D. Smith, M. Hsu, N. Bhate, *Appl. Phys. Lett.* **2010**, *97*, 234102; b) S. Martin, R. Drucker, M. Fort, *J. Geophys. Res.: Oceans* **1995**, *100*, 7027; c) S. Martin, Y. Yu, R. Drucker, *J. Geophys. Res.: Oceans* **1996**, *101*, 12111.

[42] a) M. Sleutel, J. F. Lutsko, D. Maes, A. E. Van Driessche, *Phys. Rev. Lett.* **2015**, *114*, 245501; b) A. Michaelides, K. Morgenstern, *Nat. Mater.* **2007**, *6*, 597; c) T. Mitsui, M. K. Rose, E. Fomin, D. F. Ogletree, M. Salmeron, *Science* **2002**, *297*, 1850.

[43] Y. K. Jin, Z. Y. He, Q. Guo, J. J. Wang, *Angew. Chem., Int. Ed.* **2017**, *56*, 11436.

[44] Y. K. Jin, C. Y. Wu, Y. L. Yang, J. G. Wu, Z. Y. He, J. J. Wang, *ACS Nano* **2020**, *14*, 5000.

[45] J. Chen, Z. Luo, Q. Fan, J. Lv, J. Wang, *Small* **2014**, *10*, 4693.

[46] J. Chen, R. Dou, D. Cui, Q. Zhang, Y. Zhang, F. Xu, X. Zhou, J. Wang, Y. Song, L. Jiang, *ACS Appl. Mater. Interfaces* **2013**, *5*, 4026.

[47] Y. Yu, B. Jin, M. I. Jamil, D. Cheng, Q. Zhang, X. Zhan, F. Chen, *ACS Appl. Mater. Interfaces* **2019**, *11*, 12838.

[48] T. S. Wong, S. H. Kang, S. K. Tang, E. J. Smythe, B. D. Hatton, A. Grinthal, J. Aizenberg, *Nature* **2011**, *477*, 443.

[49] H. F. Bohn, W. Federle, *Proc. Natl. Acad. Sci. U. S. A.* **2004**, *101*, 14138.

[50] B. Pokroy, A. K. Epstein, M. C. M. Persson-Gulda, J. Aizenberg, *Adv. Mater.* **2009**, *21*, 463.

[51] P. Irajizad, M. Hasnain, N. Farokhnia, S. M. Sajadi, H. Ghasemi, *Nat. Commun.* **2016**, *7*, 13395.

[52] K. Golovin, A. Dhyani, M. D. Thouless, A. Tuteja, *Science* **2019**, *364*, 371.

[53] a) M. D. Thouless, A. G. Evans, M. F. Ashby, J. W. Hutchinson, *Acta Metall.* **1987**, *35*, 1333; b) Z. Suo, J. W. Hutchinson, *Int. J. Fract.* **1990**, *43*, 1; c) M. D. Thouless, *J. Vac. Sci. Technol., A* **1991**, *9*, 2510.

[54] a) M. Paven, P. Papadopoulos, S. Schottler, X. Deng, V. Mailander, D. Vollmer, H. J. Butt, *Nat. Commun.* **2013**, *4*, 2512; b) J. B. Boreyko, C.-H. Chen, *Phys. Rev. Lett.* **2009**, *103*, 174502.

[55] Y. Hou, M. Yu, Y. Shang, P. Zhou, R. Song, X. Xu, X. Chen, Z. Wang, S. Yao, *Phys. Rev. Lett.* **2018**, *120*, 075902.

[56] J. Liu, H. Guo, B. Zhang, S. Qiao, M. Shao, X. Zhang, X.-Q. Feng, Q. Li, Y. Song, L. Jiang, J. Wang, *Angew. Chem., Int. Ed.* **2016**, *55*, 4265.

[57] a) V. Bergeron, D. Bonn, J. Y. Martin, L. Vovelle, *Nature* **2000**, *405*, 772; b) D. Bartolo, C. Josserand, D. Bonn, *J. Fluid Mech.* **2005**, *545*, 329; c) M. Reyssat, D. Richard, C. Clanet, D. Quéré, *Faraday Discuss.* **2010**, *146*, 19.

[58] a) Y. Liu, L. Moevius, X. Xu, T. Qian, J. M. Yeomans, Z. Wang, *Nat. Phys.* **2014**, *10*, 515; b) Y. Liu, M. Andrew, J. Li, J. M. Yeomans, Z. Wang, *Nat. Commun.* **2015**, *6*, 10034.

[59] a) S. Wu, Y. Du, Y. Alsaid, D. Wu, M. Hua, Y. Yan, B. Yao, Y. Ma, X. Zhu, X. He, *Proc. Natl. Acad. Sci. U. S. A.* **2020**, *117*, 11240; b) S. Dash, J. de Ruiter, K. K. Varanasi, *Sci. Adv.* **2018**, *4*, eaat0127; c) X. Yin, Y. Zhang, D. Wang, Z. Liu, Y. Liu, X. Pei, B. Yu, F. Zhou, *Adv. Funct. Mater.* **2015**, *25*, 4237; d) S. Jung, L. P. Raj, A. Rahimi, H. Jeong, R. S. Myong, *Aerosp. Sci. Technol.* **2020**, *106*, 106174.

Xiaoteng Zhou is a Ph.D. student in Prof. Hans-Jürgen Butt's group at the Max Planck Institute for Polymer Research (MPIP). He received his master degree from Tsinghua University in 2016, and bachelor degree from University of Science and Technology, Beijing in 2012. His current research focuses on wetting phenomenon and liquid-repellent surfaces.

Yuling Sun now works as a Post-Doctoral Research Fellow in Prof. Mischa Bonn's group at the Max-Planck Institute for Polymer Research. She completed her Ph.D. at Tsinghua University (Prof. Yanbin Huang Group) in 2018. Dr. Sun's research interest focuses on designing antifreeze proteins anti-icing surface, studying the antifreezing mechanism of antifreeze proteins, and development of novel cryoprotectants for cells, tissues, or organs.

Jie Liu currently works as a Post-Doctoral Research Fellow in Prof. Hans-Jürgen Butt's group at the Max-Planck Institute for Polymer Research. He performed his Ph.D. research in Prof. Jianjun Wang's group from 2012 to 2017 in ICCAS. Dr. Liu's research interest focuses on the molecular-level understanding and control of ice formation, dynamical properties of water droplets for diverse applications, and fabrication of functional liquid-repellent surfaces.